# Folding-model analysis of inelastic $\alpha+{}^{12}$C scattering at medium energies, and the isoscalar transition strengths of the cluster states of ${}^{12}$C

Do Cong Cuong and Dao T. Khoa[*]

*Institute for Nuclear Science and Technology, VINATOM, 179 Hoang Quoc Viet Road, Hanoi, Vietnam*

Yoshiko Kanada-En'yo

*Department of Physics, Kyoto University, Kyoto 606-8502, Japan*
(Received 16 October 2013; published 17 December 2013)

**Background:** The (spin and isospin zero) $\alpha$-particle is an efficient projectile for the excitation of the isoscalar, natural-parity states of ${}^{12}$C. Among those states that have pronounced $\alpha$-cluster structure, the Hoyle state ($0_2^+$ state at 7.65 MeV) has been observed in many $(\alpha,\alpha')$ experiments while the second $2^+$ state of ${}^{12}$C, predicted at $E_x \approx 10$ MeV as an excitation of the Hoyle state, has not been observed until a recent high-precision experiment of the $\alpha + {}^{12}$C scattering at $E_\alpha = 386$ MeV. A plausible reason is a strong population of the narrow $3_1^-$ state at 9.64 MeV and broad $0_3^+$ resonance at 10.3 MeV that hinders the weak $2_2^+$ peak in the $(\alpha,\alpha')$ spectrum.

**Purpose:** The accurate determination of the electric $E\lambda$ transition strengths of the isoscalar states of ${}^{12}$C, including an $E2$ component at $E_x \approx 10$ MeV that can be assigned to the $2_2^+$ state, based on a detailed folding-model + coupled-channels analysis of the $(\alpha,\alpha')$ data measured at $E_\alpha = 240$ and 386 MeV.

**Method:** The complex optical potential and inelastic form factor given by the folding model for the $\alpha + {}^{12}$C scattering are used to calculate the $(\alpha,\alpha')$ cross sections for the known isoscalar states of ${}^{12}$C in an elaborate coupled-channels approach. The strengths of the form factors for these states are then fine tuned against the $(\alpha,\alpha')$ data to deduce the corresponding $E\lambda$ transition strengths.

**Results:** A significant $E2$ transition strength has been obtained for the $2_2^+$ state from the present analysis of the $(\alpha,\alpha')$ data measured at $E_\alpha = 240$ and 386 MeV. The $E\lambda$ transition strengths of the $0_2^+$, $3_1^-$, $0_3^+$, and $1_1^-$ states were also carefully deduced, and some difference from the results of earlier analyses has been found and qualitatively understood.

**Conclusion:** Despite a strong hindrance by the $3_1^-$ and $0_3^+$ excitations, the presence of the $2_2^+$ state in the $(\alpha,\alpha')$ spectra measured at $E_\alpha = 240$ and 386 MeV has been consistently confirmed by the present folding-model + coupled-channels analysis.

## I. INTRODUCTION

The excited states of ${}^{12}$C at energies near the $\alpha$-decay threshold have attracted broad interest recently [1,2] because of the dominant $\alpha$-cluster structure established in several cases, like that of the isoscalar $0_2^+$ state at 7.65 MeV in ${}^{12}$C (known as the Hoyle state that plays a vital role in the carbon synthesis). Although a three-$\alpha$-cluster structure of the Hoyle state was shown more than three decades ago by the resonating group method (RGM) calculations [3–5], an interesting $\alpha$-condensate scenario [2] for this state has been suggested recently [6,7], where three $\alpha$ clusters were shown to condense into the lowest $S$ state of their potential. Nevertheless, a more complicated structure of the Hoyle state is still being discussed [8,9]. Given a strongly nonspherical shape of ${}^{12}$C in the Hoyle state, an excited rotational band with the angular momentum $J^\pi = 2^+, 4^+, \ldots$ built upon the Hoyle state was suggested more than 50 years ago by Morinaga [10]. In the $\alpha$-condensate scenario, where the Hoyle state is the lowest $S$ state, it is also natural that the next level in the potential containing three $\alpha$ particles should be a $2^+$ state formed by promoting an $\alpha$-particle from the $S$ to the $D$ level. The second $2^+$ state of ${}^{12}$C has been predicted by several structure models [11–14] at the

excitation energy around 10 MeV, i.e., about 2 MeV above the $\alpha$-decay threshold, with a pronounced ${}^8$Be $+ \alpha$ structure [1].

Because such an interesting structure has been predicted for the $2_2^+$ state of ${}^{12}$C, numerous experimental studies over the years have been aimed to detect it in the measured spectra of different reactions involving ${}^{12}$C (see, e.g., Refs. [15–20]). The experimental observation of the $2_2^+$ state of ${}^{12}$C would be very important for a deeper understanding of the structure of the Hoyle state. In particular, the measured excitation energy would allow us to determine the moment of inertia and deformation of ${}^{12}$C being in the Hoyle state [10,20,21]. Although some experimental evidence for a broad $2^+$ resonance was found in the aforementioned experiments that might be assigned to the $2_2^+$ state of ${}^{12}$C, a clear identification of this state could be made in the high-precision experiments on the inelastic $\alpha$ scattering [22] and photodissociation of carbon [23,24]. The plausible explanations for the difficulty in identifying the $2_2^+$ state are as follows.

(i) Like all states above the $\alpha$-decay threshold, the $2_2^+$ state is unstable against the disintegration of ${}^{12}$C* into three $\alpha$ particles and is, therefore, a short-lived resonance that is difficult to locate [9,21].

(ii) There is always a strong population of the narrow $3_1^-$ state at 9.64 MeV and broad $0_3^+$ resonance at

_____
[*]khoa@vinatom.gov.vn

10.3 MeV that hinder the $2_2^+$ peak at about 10 MeV in the excitation spectrum of $^{12}$C [18].

We believe that the latter is the main reason why it was so difficult to observe the $2_2^+$ state of $^{12}$C in the inelastic $(\alpha,\alpha')$ or $(p,p')$ scattering. Our first attempt to investigate this puzzled situation based on a detailed folding-model analysis of the inelastic $\alpha + ^{12}$C scattering data at 240 MeV [25] was done in Ref. [26], where a weak $2_2^+$ peak at $E_x \approx 9$–10 MeV has been shown to be strongly hindered by the $3_1^-$ peak at 9.64 MeV and $0_3^+$ resonance at 10.3 MeV. Given a recent observation of the $2_2^+$ state of $^{12}$C in the high-precision $(\alpha,\alpha')$ measurement at $E_\alpha = 386$ MeV [22], as well as its location and the $E2$ strength determined accurately from the photodissociation experiment [23,24], we found it necessary to carry out again a consistent folding-model analysis of the inelastic $\alpha + ^{12}$C scattering data measured at $E_\alpha = 240$ and 386 MeV using the nuclear transition densities predicted by the antisymmetrized molecular dynamics (AMD) calculation [13]. Our goal is not only to give a microscopic description of the $(\alpha,\alpha')$ data at these two energies and try to deduce the $E2$ transition strength of the $2_2^+$ state of $^{12}$C from the experimental cross section at the excitation energy $E_x \approx 10$ MeV, but also to understand why the $2_2^+$ state could not be identified at this energy by the original multipole decomposition analysis of the 240-MeV $(\alpha,\alpha')$ data [25].

## II. THEORETICAL MODELS

### A. The double-folding model

The generalized double-folding model of Ref. [27] was used to evaluate the complex $\alpha + ^{12}$C optical potential (OP) and inelastic scattering form factor (FF) from the Hartree-Fock-type matrix elements of the (complex) effective nucleon-nucleon $(NN)$ interaction between the projectile nucleon $i$ and target nucleon $j$,

$$U_{A \to A^*} = \sum_{i \in \alpha; j \in A, j' \in A^*} [\langle ij'|v_{\mathrm{D}}|ij\rangle + \langle ij'|v_{\mathrm{EX}}|ji\rangle], \quad (1)$$

where $A$ and $A^*$ denote the target in the entrance and exit channels of the $(\alpha,\alpha')$ scattering, respectively. Thus, Eq. (1) gives the (diagonal) OP if $A^* = A$ and (nondiagonal) inelastic scattering FF if otherwise. The (local) direct term is evaluated by the standard double-folding integration,

$$U_{\mathrm{D}}(E,\boldsymbol{R}) = \int \rho_\alpha(\boldsymbol{r}_\alpha)\rho_A(\boldsymbol{r}_A)v_{\mathrm{D}}(E,\rho,s)d^3r_\alpha d^3r_A,$$
$$s = \boldsymbol{r}_A - \boldsymbol{r}_\alpha + \boldsymbol{R}. \quad (2)$$

The antisymmetrization gives rise to the exchange term in Eq. (1), which is, in general, nonlocal. An accurate local equivalent exchange potential can be obtained [27,28] using the local WKB approximation [29] for the change in relative motion induced by the exchange of spatial coordinates of each interacting nucleon pair,

$$U_{\mathrm{EX}}(E,\boldsymbol{R}) = \int \rho_\alpha(\boldsymbol{r}_\alpha,\boldsymbol{r}_\alpha+s)\rho_A(\boldsymbol{r}_A,\boldsymbol{r}_A-s)v_{\mathrm{EX}}(E,\rho,s)$$
$$\times \exp\left[\frac{i\boldsymbol{K}(R)s}{M}\right]d^3r_\alpha d^3r_A. \quad (3)$$

Here $\boldsymbol{K}(R)$ is the local momentum of relative motion determined as

$$K^2(R) = \frac{2\mu}{\hbar^2}[E_{\mathrm{c.m.}} - \mathrm{Re}U_0(E,R) - V_C(R)], \quad (4)$$

where $\mu$ is the reduced mass, $M = 4A/(4+A)$, $E_{\mathrm{c.m.}}$ is the scattering energy in the center-of-mass (c.m.) frame, and $U_0(E,R)$ and $V_C(R)$ are the nuclear and Coulomb parts of the *real* OP, respectively. The calculation of $U_{\mathrm{EX}}$ is done iteratively based on a density-matrix expansion method [27,30]. We have used here a realistic local approximation for the *transition* density matrix suggested by Love [31]. The recoil correction to the exchange term (3) suggested by Carstoiu and Lassaut [32] has been taken into account.

Among different choices of the effective $NN$ interaction, a density-dependent version of the M3Y-Paris interaction (dubbed as CDM3Y6 interaction [33]) has been used quite successfully in the folding-model analyses of the elastic and inelastic $\alpha$-nucleus scattering [28]. The density-dependent parameters of the CDM3Y6 interaction were carefully adjusted in the Hartree-Fock scheme to reproduce the saturation properties of nuclear matter [33]. To avoid a phenomenological choice of the imaginary parts of the OP and inelastic FF, we have supplemented the M3Y-Paris interaction with a realistic *imaginary* density dependence [34] for the folding calculation of the imaginary parts of the OP and inelastic FF. The parameters of the imaginary density dependence have been deduced at each energy based on the Brueckner Hartree-Fock results for the nucleon OP in nuclear matter by Jeukenne, Lejeune, and Mahaux (the well-known JLM potential [35]). The explicit density-dependent parameters of the (complex) CDM3Y6 interaction for the $\alpha$-nucleus scattering at the energies $E_\alpha = 240$ and 386 MeV are given in Ref. [34].

The key quantity in our folding-model analysis of the inelastic $\alpha$-nucleus scattering is the inelastic FF that contains all the structure information of the nuclear state under study. Given an accurate choice of the effective $NN$ interaction, the present double-folding approach can be applied successfully to study the inelastic $\alpha + ^{12}$C scattering only if the realistic nuclear densities were used in the folding calculation (2)–(3). In our earlier studies, the nuclear densities given by the RGM wave functions [4] have been used in the folding-model analysis to probe the $E0$ transition strength of the Hoyle state [36], and other isoscalar excitations of $^{12}$C, like $2_1^+$ (4.44 MeV), $3_1^-$ (9.64 MeV), $0_3^+$ (10.3 MeV), and $1_1^-$ (10.84 MeV) states [37]. Like Ref. [26], the nuclear densities given by the AMD approach [13] have been used in the present folding-model analysis of the inelastic $\alpha + ^{12}$C scattering at $E_\alpha = 240$ and 386 MeV.

### B. The AMD nuclear transition densities in the present folding-model analysis

The AMD approach was proven to give quite realistic description of the structure of the low-lying states in light nuclei, where both the cluster and shell-model-like states are consistently reproduced [13]. In the present work, the isoscalar states of $^{12}$C are generated by the AMD approach using the method of variation after the spin-parity projection. The main structure properties of these states are summarized in Table I.

TABLE I. Excitation energies and $E\lambda$ transition strengths of the IS states of $^{12}$C under study. The calculated values are the AMD results [13], and the best-fit transition rates are given by the present folding-model + CC analysis. $M(E\lambda)$ is given in $e$ fm$^{\lambda+2}$ for the $0^+$ and $1^-$ states.

| $J^\pi$ | $\langle r^2\rangle^{1/2}_{\text{calc}}$ (fm) | $E_{\text{calc}}$ (MeV) | $E_{\text{exp}}$ (MeV) | Transition | Calc. ($e^2$ fm$^{2\lambda}$) | Best-fit ($e^2$ fm$^{2\lambda}$) | Exp. ($e^2$ fm$^{2\lambda}$) | Ref. |
|---|---|---|---|---|---|---|---|---|
| $2^+_1$ | 2.668 | 4.5 | 4.44 | $B(E2; 2^+_1 \to 0^+_1)$ | 8.4 | $8.4 \pm 1.5$ | $7.4 \pm 0.2$ | [22] |
| | | | | | | | $7.7 \pm 1.0$ | [25] |
| | | | | | | | $8.0 \pm 0.8$ | [39] |
| | | | | $B(E2; 2^+_1 \to 4^+_1)$ | 28.5 | | | |
| $0^+_2$ | 3.277 | 8.1 | 7.65 | $M(E0; 0^+_2 \to 0^+_1)$ | 6.6 | $4.5 \pm 0.5$ | $3.7 \pm 0.2$ | [25] |
| | | | | | | | $5.4 \pm 0.2$ | [40] |
| | | | | $B(E2; 0^+_2 \to 2^+_1)$ | 25.5 | | $13.0 \pm 2.0$ | [41] |
| | | | | $B(E3; 0^+_2 \to 3^-_1)$ | 3122 | | | |
| | | | | $M(E0; 0^+_2 \to 0^+_3)$ | 16.7 | | | |
| | | | | $M(E1; 0^+_2 \to 1^-_1)$ | 12.5 | | | |
| $3^-_1$ | 3.139 | 10.8 | 9.64 | $B(E3; 3^-_1 \to 0^+_1)$ | 74.4 | $59.5 \pm 3.2$ | $35.9 \pm 1.4$ | [22] |
| | | | | | | | $34.3 \pm 5.7$ | [25] |
| | | | | | | | $87.1 \pm 1.3$ | [42] |
| | | | | $B(E3; 3^-_1 \to 2^+_2)$ | 136.7 | | | |
| | | | | $M(E1; 3^-_1 \to 2^+_2)$ | 3.71 | | | |
| $0^+_3$ | 3.985 | 10.7 | 10.3 | $M(E0; 0^+_3 \to 0^+_1)$ | 2.3 | $2.9 \pm 0.3$ | $3.0 \pm 0.2$ | [25] |
| | | | | $B(E2; 0^+_3 \to 2^+_2)$ | 1553 | | | |
| $2^+_2$ | 3.993 | 10.6 | 9.84 | $B(E2; 2^+_2 \to 0^+_1)$ | 0.4 | $0.6 \pm 0.1$ | $0.37 \pm 0.02$ | [22] |
| | | | 10.13 | | | | $1.57 \pm 0.14$ | [23,24] |
| | | | | $B(E2; 2^+_2 \to 0^+_2)$ | 102 | | | |
| | | | | $B(E2; 2^+_2 \to 4^+_1)$ | 13.5 | | | |
| | | | | $B(E2; 2^+_2 \to 4^+_2)$ | 1071 | | | |
| $1^-_1$ | 3.424 | 12.6 | 10.84 | $M(E1; 1^-_1 \to 0^+_1)$ | 1.58 | $0.34 \pm 0.04$ | $0.31 \pm 0.04$ | [25] |
| | | | | $M(E1; 1^-_1 \to 2^+_2)$ | 3.73 | | | |
| | | | | $B(E3; 1^-_1 \to 2^+_2)$ | 1679 | | | |

While the AMD prediction for the shell-model-like $2^+_1$ state is quite satisfactory in both the excitation energy and $E2$ transition strength, the predicted excitation energies for higher-lying states are larger than the experimental values. However, such a difference in the excitation energies leads only to a very small change in the kinetic energy of emitted $\alpha$ particle and does not affect significantly the inelastic $\alpha + {}^{12}$C scattering cross sections calculated in the distorted wave Born approximation (DWBA) or coupled-channels (CC) formalism. However, the strength and shape of the nuclear transition density used to evaluate the inelastic FF are the most vital inputs that affect directly the calculated $(\alpha,\alpha')$ cross section. The details of the AMD approach to the excited states of $^{12}$C are given in Ref. [13]. In the present work, the AMD nuclear transition densities enter the folding calculation in the same convention as that used in Refs. [26,27,34] so that the isoscalar (IS) transition strength for a $2^\lambda$-pole nuclear transition $|J_i\rangle \to |J_f\rangle$ is described by the reduced nuclear transition rate $B(\text{IS}\lambda; J_i \to J_f) = |M(\text{IS}\lambda; J_i \to J_f)|^2$, where the $2^\lambda$-pole transition moment is determined from the corresponding nuclear transition density as

$$M(\text{IS}\lambda; J_i \to J_f) = \int dr\, r^{\lambda+2} \rho^{(\lambda)}_{J_f,J_i}(r) \quad \text{if } \lambda \geqslant 2, \quad (5)$$

$$M(\text{IS}0; J_i \to J_f) = \sqrt{4\pi} \int dr\, r^4 \rho^{(\lambda=0)}_{J_f,J_i}(r), \quad (6)$$

$$M(\text{IS}1; J_i \to J_f) = \int dr \left( r^3 - \frac{5}{3}\langle r^2\rangle r \right) r^2 \rho^{(\lambda=1)}_{J_f,J_i}(r). \quad (7)$$

Note that the IS dipole transition moment is evaluated based on higher-order corrections to the dipole operator, with spurious c.m. oscillation subtracted [38]. The reduced electric transition rate is evaluated as $B(E\lambda; J_i \to J_f) = |M(E\lambda; J_i \to J_f)|^2$, where $M(E\lambda)$ is determined in the same way as $M(\text{IS}\lambda)$ but using the proton part of the nuclear transition density only. We discuss hereafter the transition strength in terms of $B(E\lambda)$, because this is the quantity that can be compared with the experimental data. The excitation energies and $E\lambda$ transition strengths of the excited states of $^{12}$C are given in Table I. One can see that the AMD results for the excitation energies and $E\lambda$ transition strengths between the ground state $0^+_1$ and the excited $2^+_1$, $0^+_2$, and $3^-_1$ states agree reasonably with the experimental values.

Contrary to the shell-model-like $2^+_1$ state, the $2^+_2$ state has a well-defined cluster structure (see Fig. 5 of Ref. [13]), with a more extended mass distribution that leads to the matter radius $R_\text{m} = \langle r^2\rangle^{1/2} \approx 3.99$ fm, which is even larger than that predicted for the Hoyle state. More interesting are the predicted $E2$ transitions from the Hoyle state to the $2^+_2$ state and from the $2^+_2$ state to the $4^+_2$ state, $B(E2; 0^+_2 \to 2^+_2) \approx 511\ e^2$ fm$^4$ and $B(E2; 2^+_2 \to 4^+_2) \approx 1071\ e^2$ fm$^4$, which are much stronger than the $E2$ transitions between the members of the ground-state band, $B(E2; 0^+_1 \to 2^+_1) \approx 42.5\ e^2$ fm$^4$ and $B(E2; 2^+_1 \to 4^+_1) \approx 28.5\ e^2$ fm$^4$. Thus, the $E2$ transition rates predicted by

the AMD strongly suggest that the $2_2^+$ and $4_2^+$ states should be the members of a rotational band built upon the Hoyle state. We note that the $B(E2; 0_2^+ \to 2_2^+)$ value predicted by the RGM [4] or fermion molecular dynamics calculations [43] is even larger than that given by the AMD. The direct excitation of the $2_2^+$ state from the ground state has been predicted to be very weak, with $B(E2; 0_1^+ \to 2_2^+) \approx 2 \, e^2 \, \text{fm}^4$ that is significantly smaller than the latest experimental value deduced from the photodissociation experiment $^{12}\text{C}(\gamma,\alpha)^8\text{Be}$ [23,24]. We note here that the original analysis of the photodissociation data [23] resulted in $B(E2\uparrow) \approx 3.65 \, e^2 \, \text{fm}^4$ and the total width $\Gamma \approx 0.8$ MeV for the $2_2^+$ state. However, with some more data points taken, the revised analysis of the $^{12}\text{C}(\gamma,\alpha)^8\text{Be}$ data has given $B(E2\uparrow) \approx 7.85 \, e^2 \, \text{fm}^4$ and $\Gamma \approx 2.1$ MeV [24].

Nevertheless, the newly found $B(E2\uparrow)$ value for the $2_2^+$ state is still at least 5 times weaker than the $B(E2\uparrow)$ value established for the $2_1^+$ state [39]. Therefore, the $2_2^+$ state must be a very weak (*direct*) excitation of $^{12}\text{C}$ and it is, therefore, difficult to observe this state in the inelastic hadron scattering. Although a very strong $E2$ transition has been predicted for the excitation of the $2_2^+$ state from the Hoyle state, such a two-step excitation of $^{12}\text{C}$ via the Hoyle state seems to be suppressed at the medium- and high-incident $\alpha$ energies as well as by the disintegration of the excited $^{12}\text{C}^*$ into three $\alpha$ particles. This could be also another reason for the scarcity of the experimental observation of the $2_2^+$ state. Besides a strong $E2$ transition between the Hoyle state and $2_2^+$ state discussed above, AMD also predicted very strong $E\lambda$ transitions from the Hoyle state to the $3_1^-$, $0_3^+$, and $1_1^-$ states that are about an order of magnitude larger than $E\lambda$ transitions between these states and the ground state (see Table I). To have an accurate CC scenario for the $(\alpha,\alpha')$ scattering under study, all $E\lambda$ transitions shown in Table I have been included into the present CC calculation, and the coupling scheme in Fig. 1 is, therefore, more comprehensive than that used earlier in Refs. [26,36].

In the inelastic $\alpha + {}^{12}\text{C}$ scattering experiments at $E_\alpha = 240$ [25] and 386 MeV [22], the $(\alpha,\alpha')$ cross sections have been measured accurately in small energy bins of 475 and 250 keV width, respectively, over a wide range of scattering angles and excitation energies. These data have been subjected to the multipole decomposition analysis (MDA) to disentangle contribution of different $E\lambda$ multipolarities to the excitation of $^{12}\text{C}$ in each energy bin. The MDA technique is the same as that used earlier to deduce the electric transition strengths of the IS giant resonances from the $(\alpha,\alpha')$ spectrum. As a result, the $(\alpha,\alpha')$ cross sections measured at $E_\alpha = 386$ MeV for the energy bins centered around $E_x \sim 10$ MeV were shown to contain the contribution from both the $0_3^+$ and the $2_2^+$ states of $^{12}\text{C}$ [22]. Although the $3_1^-$ state at 9.64 MeV has a very narrow width of about 34 keV, the observed $3^-$ strength is distributed over a much wider energy range of the $(\alpha,\alpha')$ spectrum that is likely associated with the energy resolution of the measurement (the energy resolution of the 386-MeV measurement is around 200 keV [22]). Given our best-fit $B(E3)$ transition strength comparable to that deduced from the $(e,e')$ experiment and a good description of the measured $3_1^-$ angular distribution by the inelastic FF obtained with the AMD transition density (see Table I and Fig. 5), we have scaled the $3_1^-$ transition density to reproduce the $E3$ strength found in each energy bin by the

MDA of the $(\alpha,\alpha')$ data [22,25] and used it to calculate the $3^-$ inelastic FF for that energy bin. The situation with the $0_3^+$ and $2_2^+$ states is more uncertain; especially, no $E2$ strength was found by the MDA of the 240-MeV data [25] in the energy bins centered around 10 MeV. Therefore, we chose not to scale the AMD transition density to the $E0$ and $E2$ strengths given by the MDA of the $(\alpha,\alpha')$ data and adopted the strength-*averaging* procedure [44], used in our earlier folding-model analysis of the $(\alpha,\alpha')$ scattering on the lead target [34] at the same incident $\alpha$ energies, to predict the strength distribution of the $0_3^+$ and $2_2^+$ states over the considered energy bins. Namely, the IS transition strength $S_{\text{AMD}} \equiv B(\text{IS}\lambda; J_i \to J_f)$, given by the AMD transition density scaled to give the best CC fit of the $(\alpha,\alpha')$ data for the $0_3^+$ or $2_2^+$ states, has been spread over the excitation energy as

$$\langle S(E) \rangle = S_{\text{AMD}} f(E - E_x), \tag{8}$$

where the adopted experimental excitation energies $E_x \approx 10.3$ and 10 MeV [22,23,25] have been used for the $0_3^+$ and $2_2^+$ states, respectively, and

$$S_{\text{AMD}} = \int_E \langle S(E') \rangle dE'. \tag{9}$$

The averaging function $f(E - E_x)$ is a Gaussian distribution,

$$f(E - E_x) = \frac{1}{\sigma\sqrt{2\pi}} \exp\left[ -\frac{1}{2}\left( \frac{E - E_x}{\sigma} \right)^2 \right], \tag{10}$$

where $\sigma$ is the standard deviation associated with the full width $\Gamma$ at half maximum as $\Gamma = 2.355\sigma$. The obtained IS transition strength distribution of the $0_3^+$ and $2_2^+$ states is shown in Fig. 2, where the adopted experimental width $\Gamma \approx 3$ MeV [22,25] has been used for the $0_3^+$ state. The total width of the $2_2^+$ state has
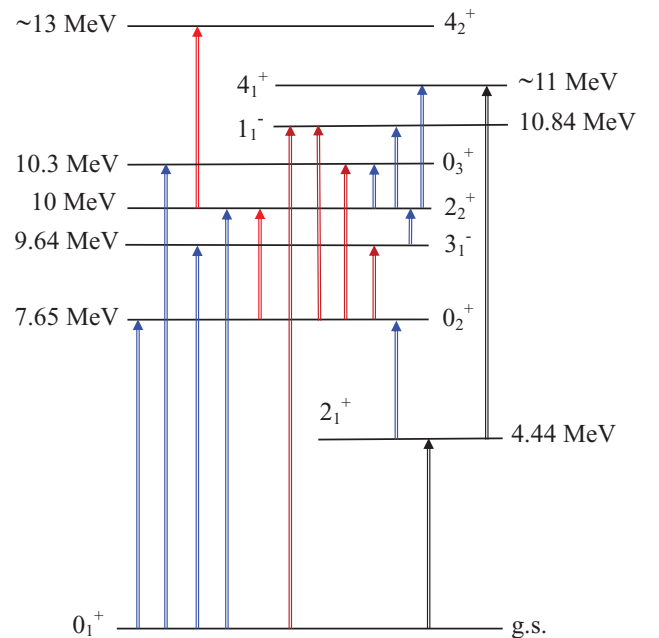


FIG. 1. (Color online) Coupling scheme used in the present CC calculation of the elastic and inelastic $\alpha + {}^{12}\text{C}$ scattering.
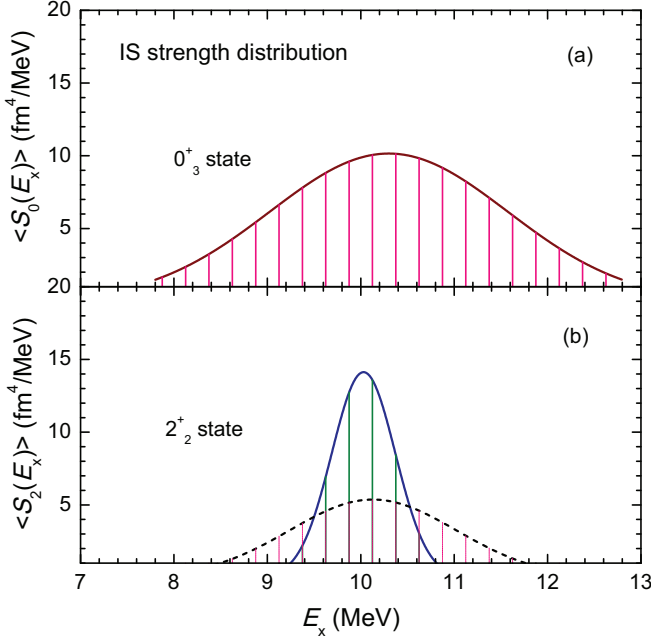
FIG. 2. (Color online) Distribution of the IS transition strength (8) of the $0_3^+$ state (a) and $2_2^+$ state (b) over the 250-keV-wide energy bins around $E_x \sim 10$ MeV used in the present folding-model + CC analysis of the $(\alpha, \alpha')$ data measured at $E_\alpha = 386$ MeV. The $E2$ strength distributions of the $2_2^+$ state based on the total width $\Gamma = 0.8$ and 2.1 MeV are shown as solid and dashed lines, respectively.

been suggested as $\Gamma \approx 0.7$–0.8 MeV by most of the experimental studies [15–18,22,23]. However, the revised analysis of the $^{12}C(\gamma, \alpha)^8Be$ data has "unambiguously" determined $\Gamma \approx 2.1 \pm 0.3$ MeV for the $2_2^+$ state [24]. To deal with such a situation, we have used two different total widths $\Gamma = 0.8$ and 2.1 MeV as the inputs for the averaging procedure (8) of the $E2$ strength of the $2_2^+$ state (see bottom panel of Fig. 2).

To obtain the inelastic scattering FF for the contribution of the considered state in each energy bin, we have used for the input of the double-folding calculation (2)–(3) the bin transition density of this state determined as

$$\rho_{bin}^{(\lambda)}(r) = \sqrt{\frac{S_{bin}}{S_{AMD}}} \rho_{AMD}^{(\lambda)}(r), \qquad (11)$$

where $\rho_{AMD}^{(\lambda)}(r)$ is the AMD transition density of the $0_3^+$ or $2_2^+$ state, scaled to give the best CC fit of the $(\alpha, \alpha')$ data, and $S_{bin}$ is the IS transition strength in the energy bin,

$$S_{bin} = \int_{E_{bin}-\Delta E}^{E_{bin}+\Delta E} \langle S(E') \rangle dE'. \qquad (12)$$

Here $E_{bin}$ is the center of the energy bin and $\Delta E$ is its half width.

## III. RESULTS AND DISCUSSION

Given the AMD transition densities calculated for different transitions between the IS states of $^{12}C$ shown in Table I, the corresponding inelastic folded FF can be used in both the DWBA and the CC analysis of the $(\alpha, \alpha')$ data. For this
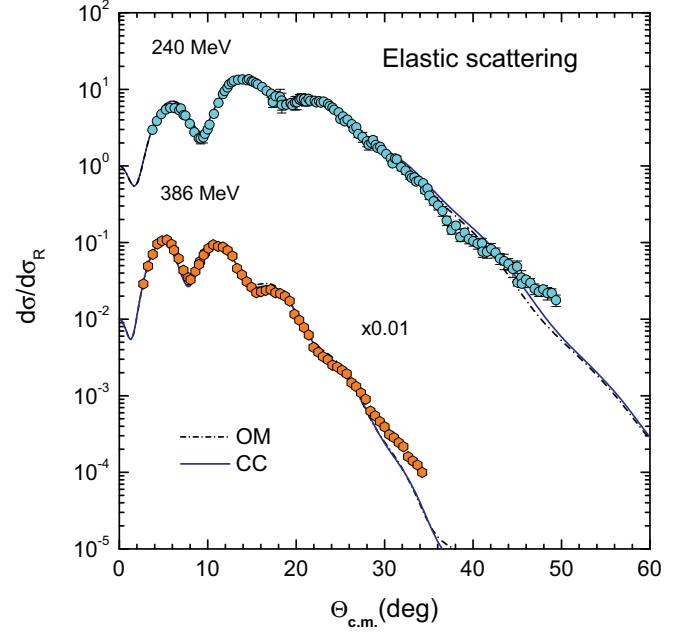


FIG. 3. (Color online) OM and CC descriptions of the elastic $\alpha + ^{12}C$ scattering data measured at $E_\alpha = 240$ MeV [25] and 386 MeV [22].

kind of analysis, an accurate determination of the distorted waves in the entrance and exit channels by the appropriately chosen OP is very crucial. In the present work, the complex OP for the entrance channel is given by the double-folding calculation (2)–(3) using the ground-state (g.s.) density of $^{12}C$ and complex CDM3Y6 density-dependent interaction. Because the exit channel of the inelastic $\alpha + ^{12}C$ scattering contains $^{12}C^*$ being in an excited (cluster) state that is generally more dilute, with the predicted $\langle r^2 \rangle^{1/2}$ radius significantly larger than $\langle r^2 \rangle_{g.s.}^{1/2} \approx 2.33$ fm (see Table I), the OP of each exit channel has been computed separately at the energy $E_\alpha - Q$, using the diagonal density of $^{12}C^*$ given by the AMD. It can be seen from the discussion below that such an elaborate treatment of the exit OP led to a better agreement of the calculated $(\alpha, \alpha')$ cross sections with the data at large angles and helped to deduce accurately the $E\lambda$ transition rates for the considered excited states (the best-fit values given in Table I).

All the optical model (OM), DWBA, and CC calculations have been performed using the code ECIS97 written by Raynal [45]. To account for the higher-order (dynamic polarization) contributions to the folded OP [27] and to fine tune the complex strength of the CDM3Y6 interaction for each energy, the real and imaginary folded OPs were scaled by the coefficients $N_R$ and $N_I$, respectively, which were adjusted to the best OM fit of the elastic scattering data (see Fig. 3). As a result, the best-fit $N_R \approx 1.05$, $N_I \approx 1.27$ and $N_R \approx 1.24$, $N_I \approx 1.38$ were obtained for $E_\alpha = 240$ and 386 MeV, respectively. We note that the imaginary strength of the CDM3Y6 interaction was tuned to the JLM results for nuclear matter and gives, therefore, only the "volume" absorption. To effectively account for the surface absorption caused by inelastic scattering and transfer reactions, etc., an enhanced $N_I$ coefficient is naturally

expected. The OM calculation using the complex folded OP gives the total reaction cross section $\sigma_R \approx 626$ and 624 mb for $E_\alpha = 240$ and 386 MeV, respectively, which are close to the $\sigma_R$ value around 640 mb given by the empirical global OP for the elastic $\alpha$-nucleus scattering [46]. These same $N_{R(I)}$ factors were used to scale the real and imaginary inelastic folded FF for the DWBA calculation, a standard method widely adopted in the folding-model + DWBA analysis of inelastic $\alpha$-nucleus scattering [25,27,47]. In the CC calculation, $N_R$ and $N_I$ must be readjusted again to account only for higher-order effects caused by the nonelastic channels not included into the CC scheme shown in Fig. 1. We have then obtained $N_R \approx 1.08$, $N_I \approx 1.18$ and $N_R \approx 1.26$, $N_I \approx 1.35$ from the CC analysis of the 240- and 386-MeV data, respectively. These $N_{R(I)}$ factors were used to scale the OP and all the (complex) inelastic folded FF's used in the present CC analysis of the $(\alpha,\alpha')$ data. From the OM and CC results shown in Fig. 3 one can see that the renormalized (complex) folded OP describes the elastic data accurately up to the large angles, thus providing the realistic distorted waves for the DWBA and CC calculations of inelastic scattering.

The DWBA and CC results for the inelastic $(\alpha,\alpha')$ scattering to the $2_1^+$ and $3_1^-$ states are compared with the experimental data in Figs. 4 and 5, respectively. One can see that all the calculated $(\alpha,\alpha')$ cross sections for the shell-model-like $2_1^+$ state agree reasonably with the data, with the CC calculation giving a slightly better fit to the 240-MeV data at large angles. The $B(E2)$ transition strength predicted by the AMD agrees
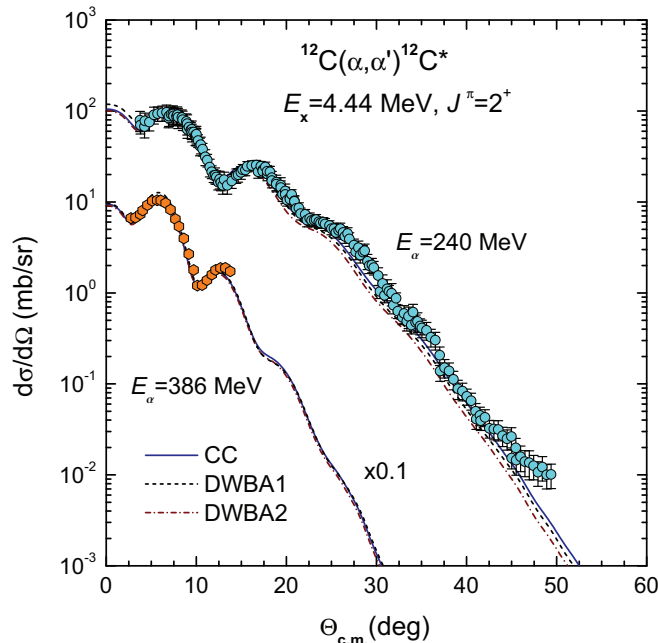
FIG. 5. (Color online) The same as Fig. 4 but for the $3_1^-$ state.

FIG. 4. (Color online) DWBA and CC descriptions of the inelastic $\alpha + {}^{12}$C scattering data for the $2_1^+$ state, measured at $E_\alpha = 240$ MeV [25] and 386 MeV [22]. The DWBA1 results were obtained using the same OP for both the entrance and the exit channels, and the DWBA2 and CC results were obtained with the OP of the exit channel computed separately at the energy $E_\alpha - Q$, using the AMD diagonal density of ${}^{12}$C*.

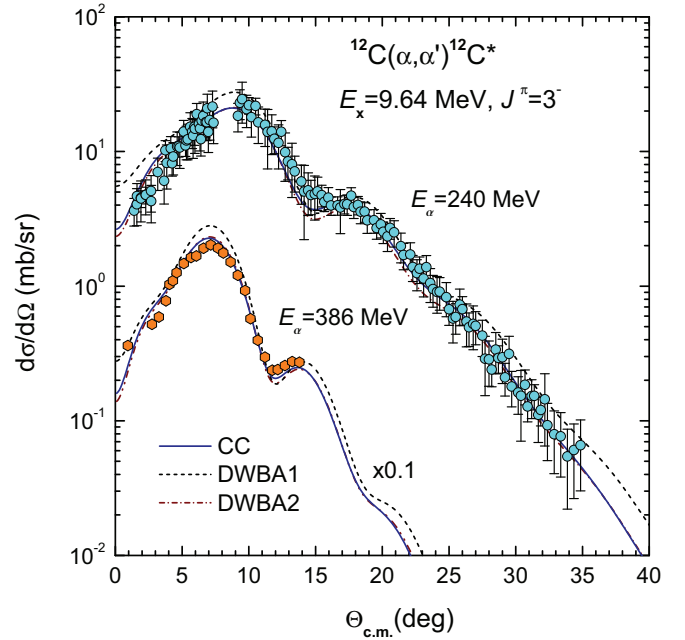well with the experimental values deduced from the $(\alpha,\alpha')$ and $(e,e')$ data [22,25,39], and the AMD nuclear transition density of the $2_1^+$ state is well suitable for the folding-model analysis. The situation with the $3_1^-$ state is quite different. The folded inelastic FF given by the original AMD transition density for the $3_1^-$ state overestimates the data in both the DWBA and the CC calculations, especially, in the standard DWBA1 calculation that uses the same OP for both the entrance and the exit channels. Using the folded FF rescaled to give a good description of the data in the CC calculation, the DWBA1 results still overestimate the data at both energies (see Fig. 5). This is obviously the reason why the best-fit $B(E3)$ values given by the (DWBA-based) MDA of the $(\alpha,\alpha')$ data [22,25] are much lower than that deduced from the $(e,e')$ data (see Table I). The more accurate DWBA2 and CC calculations, using the complex folded OP of the exit channel determined explicitly at the energy $E_\alpha - Q$ with the AMD diagonal density of ${}^{12}$C*, describe the $(\alpha,\alpha')$ data for the $3_1^-$ state much better. In this case, the rescaled AMD transition density gives the best-fit $B(E3; 3_1^- \to 0_1^+) \approx 60$ $e^2$ fm$^6$, which is closer to that deduced from the $(e,e')$ data [42]. Note that if the inelastic $3_1^-$ FF is rescaled to fit the data by the DWBA1 calculation, then the rescaled AMD transition density gives the best-fit $B(E3; 3_1^- \to 0_1^+) \approx 45$ $e^2$ fm$^6$. A straightforward explanation is that the $3_1^-$ state is more dilute, with the radius given by the diagonal density $\langle r^2 \rangle^{1/2} \approx 3.14$ fm compared to that of about 2.33 fm for the ground state. As a result, the complex folded OP for the exit channel is more absorptive at the surface and the strength of the elastic distorted waves is significantly reduced. This leads to a reduction of the calculated $(\alpha,\alpha')$ cross section as shown in Fig. 5. If one rescales, in a similar manner, the AMD transition density to give the $B(E3; 3_1^- \to 0_1^+)$ value of about 87 $e^2$ fm$^6$ deduced from the $(e,e')$ data, then the absorption of the exit channel needs to be further increased to
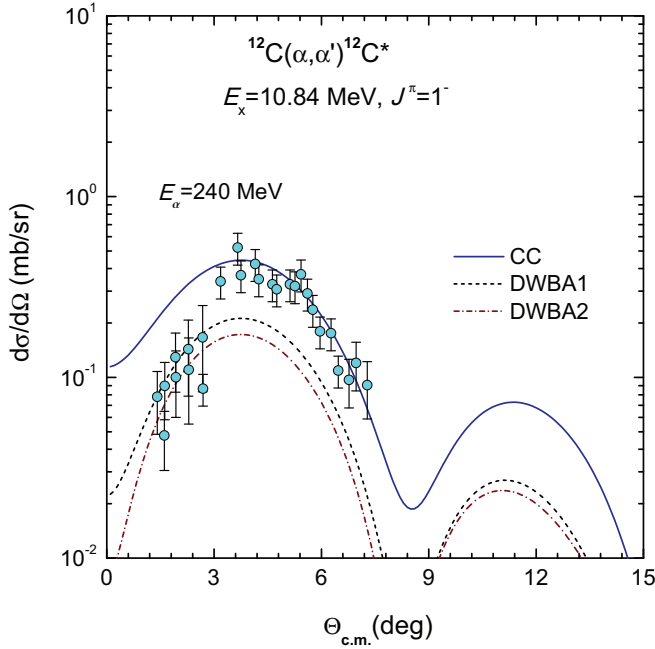
FIG. 6. (Color online) The same as Fig. 4 but for the $1_1^-$ state.



FIG. 7. (Color online) The same as Fig. 4 but for the Hoyle ($0_2^+$) state.

describe the $(\alpha,\alpha')$ data for the $3_1^-$ state by either the DWBA2 or the CC calculation. Such an important effect by the absorption in the exit channel has been discussed earlier in more details [37].

The IS dipole $1_1^-$ state at $E_x \approx 10.84$ MeV has been observed in both $(\alpha,\alpha')$ experiments at $E_\alpha = 240$ and 386 MeV. The total $(\alpha,\alpha')$ angular distribution for the $1_1^-$ state has been deduced by the MDA of the 240-MeV data [25], covering the first diffraction maximum as shown in Fig. 6. The calculated $1^-$ cross sections have a slightly broader bell shape of the first diffraction maximum, and one cannot adjust the FF strength to fit all the data points. Like the DWBA analysis of Ref. [25], we have tried to obtain the best CC fit of the calculated $1^-$ cross section to the data points at the peak of the diffraction maximum that have smaller uncertainties. This procedure implied a renormalization of the AMD transition density that gives $M(E1; 1_1^- \to 0_1^+) \approx 0.34$ $e$ fm$^3$, quite close to the DWBA results of Ref. [25] given by a collective model transition density of the $1_1^-$ state. From the DWBA and CC results shown in Fig. 6 one can see quite a strong coupling effect caused by the indirect excitation of the $1_1^-$ state via the Hoyle and $2_2^+$ states, as predicted by the AMD (see Table I and Fig. 1). Note that the direct excitation of the $1_1^-$ state has been predicted to be much stronger, with $M(E1\downarrow) \approx 1.58$ $e$ fm$^3$, and the absorption of the exit channel needs to be strongly increased [37] to describe the $(\alpha,\alpha')$ data for the $1_1^-$ state using the original AMD transition density.

The present folding-model + CC analysis of the $(\alpha,\alpha')$ scattering to the Hoyle state (see results shown in Fig. 7) has revealed interesting higher-order coupling effects that are best seen in the results obtained for the $\alpha$ energy of 240 MeV. As discussed earlier in Ref. [36], the MDA of the $(\alpha,\alpha')$ data measured at different energies has consistently found a much weaker $E0$ transition strength of the Hoyle state, with the
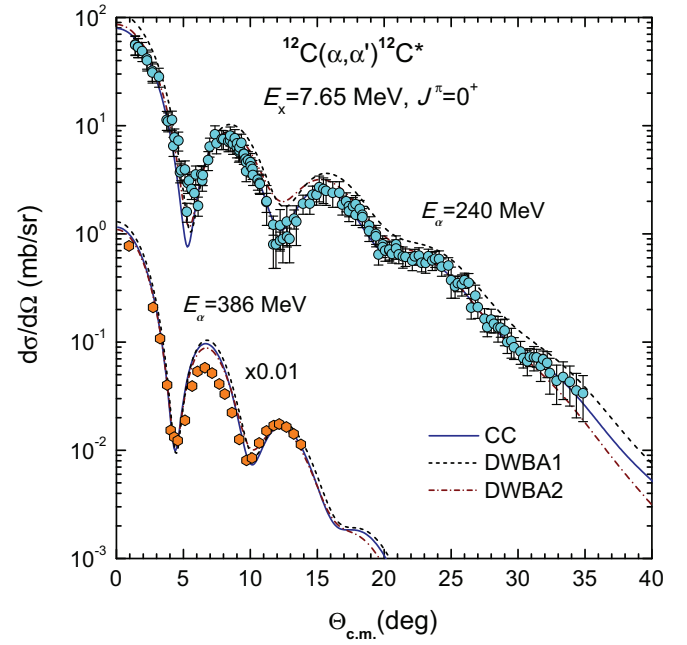
deduced $M(E0; 0_2^+ \to 0_1^+) \approx 3.6\text{–}3.8$ $e$ fm$^2$ that is about 30% weaker than the experimental value $M(E0\downarrow)_{\text{exp}} \approx 5.4$ $e$ fm$^2$ deduced from the $(e,e')$ data [40]. The DWBA1 calculation using the (rescaled) AMD transition density would give the best-fit $M(E0\downarrow) \approx 3.65$ $e$ fm$^2$, about the same as that given by the RGM transition density rescaled to fit the $(\alpha,\alpha')$ data in the DWBA [36]. The present CC calculation included all possible second-order transitions from the Hoyle state to the neighboring cluster states (see Fig. 1). In particular, very strong $E\lambda$ transitions between the Hoyle state and the $3_1^-, 0_3^+$, and $1_1^-$ states have been taken into account (see Table I). As a result, the best-fit $E0$ strength given by the folding-model + CC analysis of the 240-MeV data is $M(E0\downarrow) \approx 4.5$ $e$ fm$^2$, which is about 20% stronger than that given by the standard DWBA analysis. It is likely that a full coupled reaction channel analysis of the $(\alpha,\alpha')$ data including different breakup channels would yield the best-fit $M(E0\downarrow)$ value closer to the $(e,e')$ data, and that would physically explain the missing monopole strength of the Hoyle state in $(\alpha,\alpha')$ scattering that can be accounted for in the DWBA only by an enhanced absorption in the exit channel [36,37].

The $E0$ transition strength of the $0_3^+$ resonance has not been unambiguously determined by previous studies. For example, the RGM calculation predicted about the same $M(E0\downarrow)$ value for both the Hoyle and $0_3^+$ states [4,22], while the AMD gives a much weaker monopole strength of the $0_3^+$ state, with the ratio $M(E0; 0_3^+ \to 0_1^+)/M(E0; 0_2^+ \to 0_1^+) \approx 0.34$. The MDA of the 386-MeV data [22], using the nuclear transition densities from the collective model, gives $M(E0; 0_3^+ \to 0_1^+)/M(E0; 0_2^+ \to 0_1^+) \approx 1$. Given the CC scheme of Fig. 1, a more precise determination of the $E0$ strength of the $0_3^+$ state should be important for a realistic determination of the $E2$ strength of the $2_2^+$ state because these two cluster states
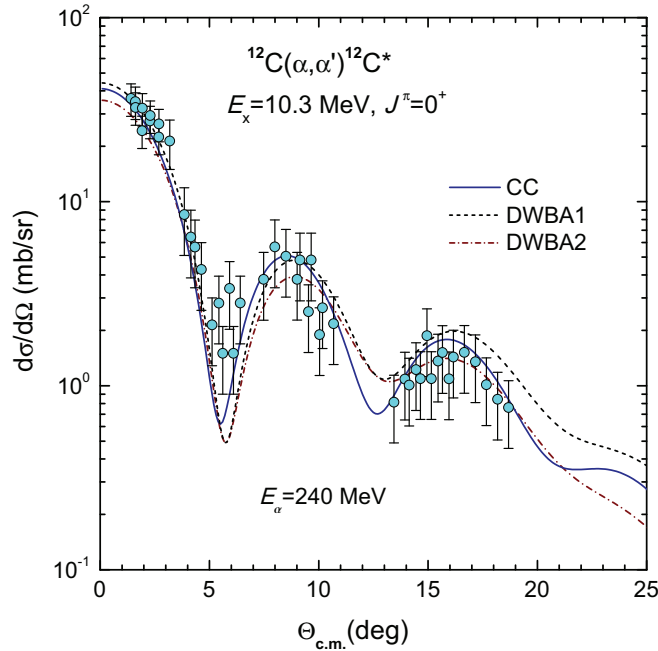
FIG. 8. (Color online) DWBA and CC descriptions of the inelastic $\alpha + {}^{12}$C scattering data for the $0_3^+$ state, measured at $E_\alpha = 240$ MeV [25]. The curves DWBA1 and DWBA2 were obtained in the same way as described in the caption of Fig. 4.


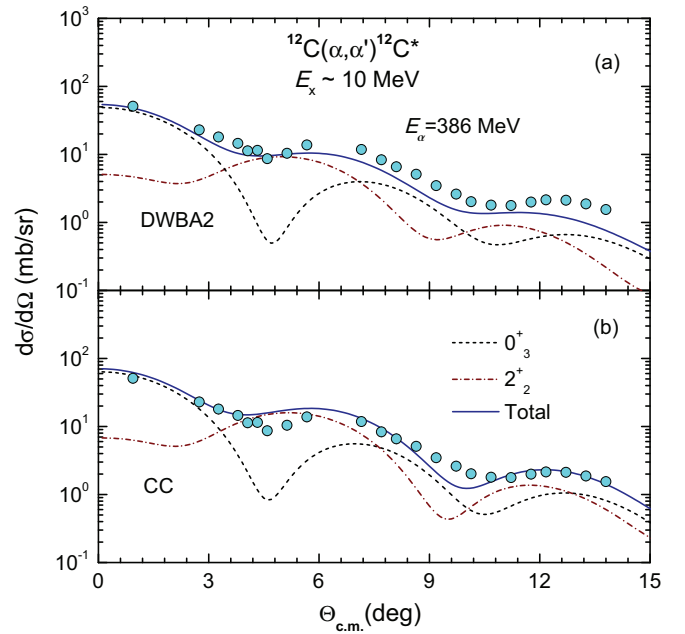
FIG. 9. (Color online) DWBA (a) and CC (b) descriptions of the inelastic $\alpha + {}^{12}$C scattering data measured at $E_\alpha = 386$ MeV for the $0_3^+$ and $2_2^+$ states [22]. The DWBA2 and CC results were obtained in the same way as described in the caption of Fig. 4. The $E2$ strength of the $2_2^+$ state has been adjusted to the best CC fit to the data, giving $B(E2\downarrow) \approx 0.6 \, e^2 \, \text{fm}^4$.

are connected by a very strong "interband" $E2$ transition with $B(E2; 0_3^+ \to 2_2^+)$ predicted by the AMD to be around $1500 \, e^2 \, \text{fm}^4$ (see Table I). Our folding-model + DWBA (CC) analysis of the 240-MeV data for the $0_3^+$ state has been done in the same manner as discussed above for the $3_1^-$ and Hoyle states, and the results are plotted in Fig. 8. The best-fit $E0$ transition strength $M(E0; 0_3^+ \to 0_1^+) \approx 2.9 \, e \, \text{fm}^2$ is close to that given by the MDA of the 240-MeV data [25]. The $(\alpha, \alpha')$ cross section calculated in the CC formalism agrees perfectly with the measured data over the whole angular range (see solid curve in Fig. 8). The DWBA1 calculation using the same inelastic FF as that used in the CC calculation gives a poorer description of the data points at large angles, like the DWBA results of Ref. [25]. The DWBA2 calculation improves the agreement of the calculated $0_3^+$ cross section with the data, but the fit is still worse than that given by the CC calculation. Thus, the best description of the $(\alpha, \alpha')$ data measured at $E_\alpha = 240$ MeV for both the Hoyle and $0_3^+$ states has been consistently given by the present folding-model + CC analysis, using the AMD transition densities rescaled to give $M(E0\downarrow) \approx 4.5$ and $2.9 \, e \, \text{fm}^2$, respectively. This result gives the ratio $M(E0; 0_3^+ \to 0_1^+)/M(E0; 0_2^+ \to 0_1^+) \approx 0.64$.

The MDA of the $(\alpha, \alpha')$ data measured at $E_\alpha = 386$ MeV has shown a broad $0_3^+$ resonance and a narrower $2_2^+$ state centered at the excitation energies $E_x \approx 9.93$ and 9.84 MeV, respectively. After the subtraction of the known $0_2^+$, $3_1^-$, and $1_1^-$ peaks, the total $(\alpha, \alpha')$ angular distribution deduced for the wide bump centered at $E_x \approx 10$ MeV has been shown [22] to contain only the coherent contributions from the $2_2^+$ and $0_3^+$ states (see Fig. 9). Given the $E0$ strength of the $0_3^+$ state accurately determined above in the analysis of the 240-MeV

data, the $E2$ strength of the $2_2^+$ state remains the only parameter in the present analysis of the 386-MeV $(\alpha, \alpha')$ data. Thus, the strength of the $2_2^+$ folded FF was adjusted to the best CC description of the $(\alpha, \alpha')$ angular distribution, as shown in Fig. 9. Although the $\alpha$ energy of 386 MeV can be considered as high enough for the validity of the DWBA, very strong $E\lambda$ transitions between the $2_2^+$ state and other cluster states of ${}^{12}$C (see Table I and Fig. 1) have led to quite a significant CC effect. From the DWBA2 and CC results shown in Fig. 9 one can see that the calculated $(\alpha, \alpha')$ cross section for the $2_2^+$ state is indeed enhanced by the indirect excitation of the $2_2^+$ state via other cluster states. As a result, the best description of the $(\alpha, \alpha')$ data measured at $E_\alpha = 386$ MeV for the $2_2^+$ and $0_3^+$ states is given by the folding-model + CC calculation using the $2_2^+$ transition density rescaled to give $B(E2; 2_2^+ \to 0_1^+) \approx 0.6 \, e^2 \, \text{fm}^4$, which is about 50% larger than that predicted by the AMD calculation (see Table I). Although in a fine agreement with $B(E2\downarrow)_{\text{exp}} \approx 0.73 \, e^2 \, \text{fm}^4$ given by the original analysis of the photodissociation data [23], the best-fit $B(E2\downarrow)$ value of about $0.6 \, e^2 \, \text{fm}^4$ turns out to be significantly lower than $B(E2\downarrow)_{\text{exp}} \approx 1.57 \, e^2 \, \text{fm}^4$, a value deduced from the revised analysis of the ${}^{12}$C$(\gamma, \alpha)^8$Be data [24]. However, if one sticks to a simple DWBA scenario like that in Ref. [22] and adjust the $E0$ strength of the $0_3^+$ state to fit the data shown in Fig. 9, keeping the $B(E2\downarrow)$ transition rate of the $2_2^+$ state fixed at a value around $0.4 \, e^2 \, \text{fm}^4$, then the best-fit $E0$ strength of the $0_3^+$ state would increase and the agreement between the calculation and experiment shown in Fig. 8 would deteriorate. Thus, a consistent folding-model + CC description of the $(\alpha, \alpha')$ data
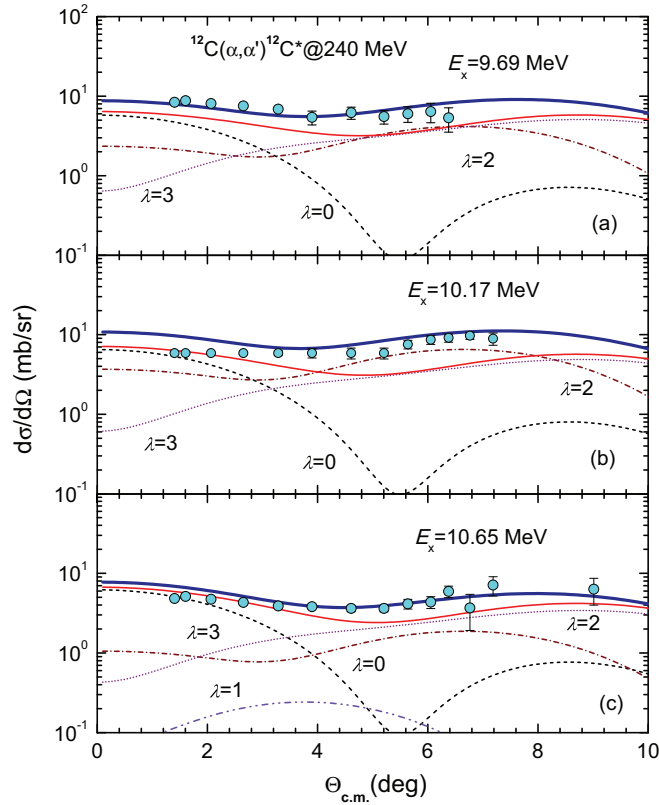
FIG. 10. (Color online) Differential $(\alpha,\alpha')$ cross sections measured at $E_\alpha = 240$ MeV [25,48] for the 475-keV-wide energy bins centered at $E_x = 9.69$ MeV (a), 10.17 MeV (b), and 10.65 MeV (c), and the CC results given by the contributions of different $2^\lambda$-pole transition strengths. The total cross sections obtained with and without the contribution from the $2_2^+$ state are shown as the thick (blue) and thin (red) solid lines, respectively.

measured at both energies $E_\alpha = 240$ and 386 MeV shown in Figs. 8 and 9, respectively, has been achieved with the AMD transition densities rescaled to give the best-fit $E2$ and $E0$ strengths tabulated in Table I for the $2_2^+$ and $0_3^+$ states.

A natural question now is why the $2_2^+$ state has not been observed at $E_x \approx 10$ MeV in the $(\alpha,\alpha')$ experiment at $E_\alpha = 240$ MeV. In fact, the MDA of the 240-MeV $(\alpha,\alpha')$ data has established a $2^+$ peak at $E_x \approx 11.46$ MeV, with the width of about 430 keV and $B(E2\downarrow) \approx 0.5$ $e^2$ fm$^4$, that could be assigned to the $2_2^+$ state [25]. Given the realistic $E\lambda$ strengths of the IS states found above in our folding-model + CC analysis of both data sets, we decided to look again at the 240-MeV $(\alpha,\alpha')$ data measured for several energy bins around 10 MeV [25,48]. As discussed in Sec. II B, the $3^-$ transition strength found in each energy bin by the MDA of the 240-MeV $(\alpha,\alpha')$ data [25] was used to scale the AMD transition density to obtain the $3^-$ inelastic FF of the bin. The best-fit $E\lambda$ transition strengths found above for the $2_2^+$, $0_3^+$, and $1_1^-$ states were distributed over the energy bins by the averaging procedure (8)–(10) for the determination of the corresponding inelastic FF of the bin. We note that a width $\Gamma = 315$ keV [17] has been assumed in the averaging of the $E1$ strength of the $1_1^-$ state. The CC description of the 240-MeV $(\alpha,\alpha')$ data measured
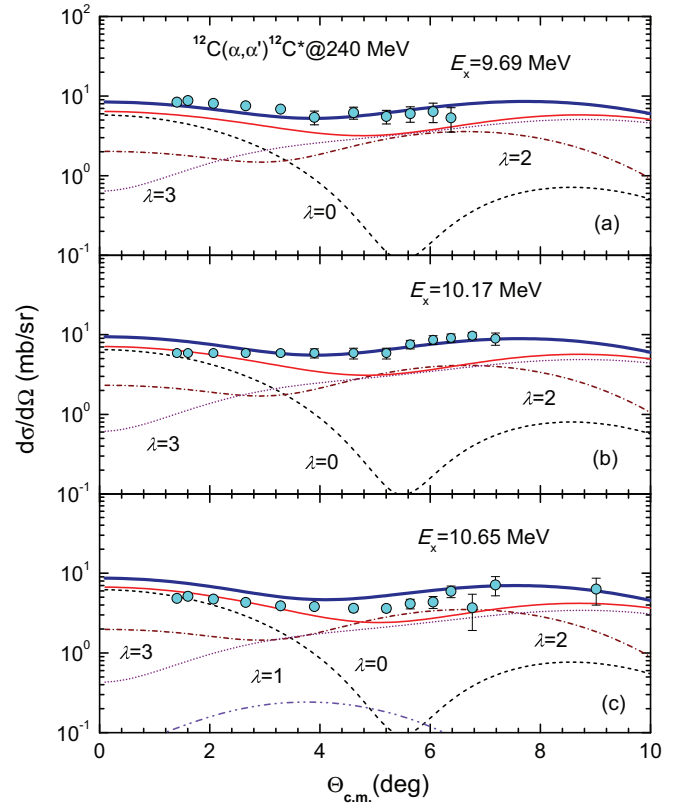
FIG. 11. (Color online) The same as Fig. 10 but with the $E2$ strength of the $2_2^+$ state distributed over a wider energy range spanned by the total width $\Gamma = 2.1$ MeV.

for three energy bins closest to $E_x = 10$ MeV is shown in Fig. 10. From the calculated total cross section with (thick solid lines) and without the contribution from the $2_2^+$ state (thin solid lines) one can see clearly that the $E2$ strength of the $2_2^+$ state is indeed present in these energy bins. Because the CC description of the $(\alpha,\alpha')$ data shown in Fig. 10 has been obtained without any further readjusting of the $E\lambda$ strengths of the involved cluster states, we conclude that the presence of the $2_2^+$ state at the energy near 10 MeV has been found by the present folding-model + CC analysis of the $(\alpha,\alpha')$ data at $E_\alpha = 240$ MeV. Such a subtle effect could not be resolved in the original MDA of the 240-MeV $(\alpha,\alpha')$ data.

Owing to the uncertainty in the measured total width of the $2_2^+$ state discussed above in Sec. II B, the $E2$ strength distribution of this state was built up in two distinct scenarios by the averaging procedure (8) using the total width $\Gamma = 0.8$ and 2.1 MeV for this state. To assess the effect by the width of the $E2$ strength distribution, we have calculated again the 240-MeV $(\alpha,\alpha')$ cross sections for the same three energy bins as in Fig. 10 but using the $E2$ strength of the $2_2^+$ state distributed over a wider energy range spanned by the total width $\Gamma = 2.1$ MeV. From the results shown in Fig. 11, one can see a better agreement of the CC results with the data in the energy bins centered at $E_x = 9.69$ and 10.17 MeV, while the agreement with the data in the bin centered at 10.65 MeV slightly worsens. A clear presence of the $2_2^+$ state at the energy near 10 MeV
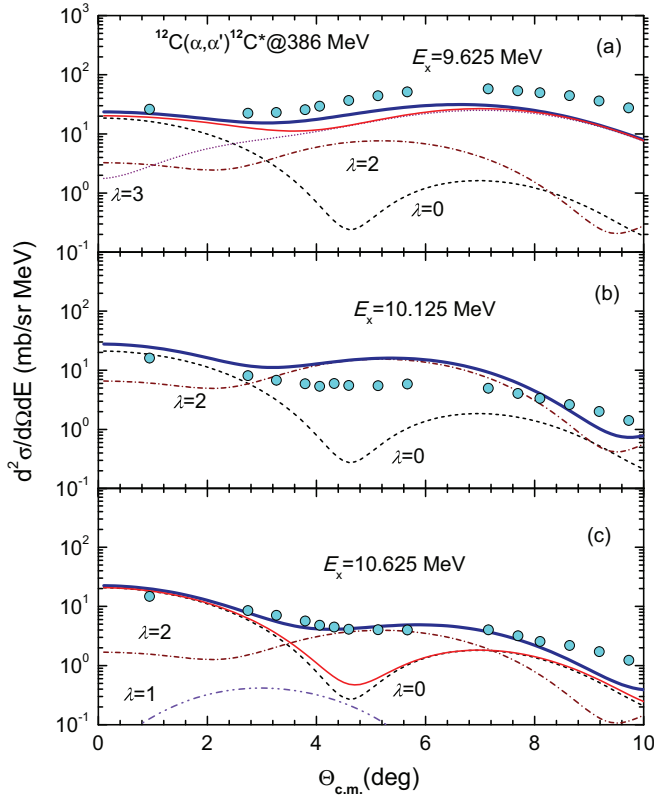
FIG. 12. (Color online) Double-differential $(\alpha,\alpha')$ cross sections measured at $E_\alpha = 386$ MeV [22] for the 250-keV-wide energy bins centered at $E_x = 9.625$ MeV (a), 10.125 MeV (b), and 10.625 MeV (c), in comparison with the CC results in the same way as in Fig. 10.
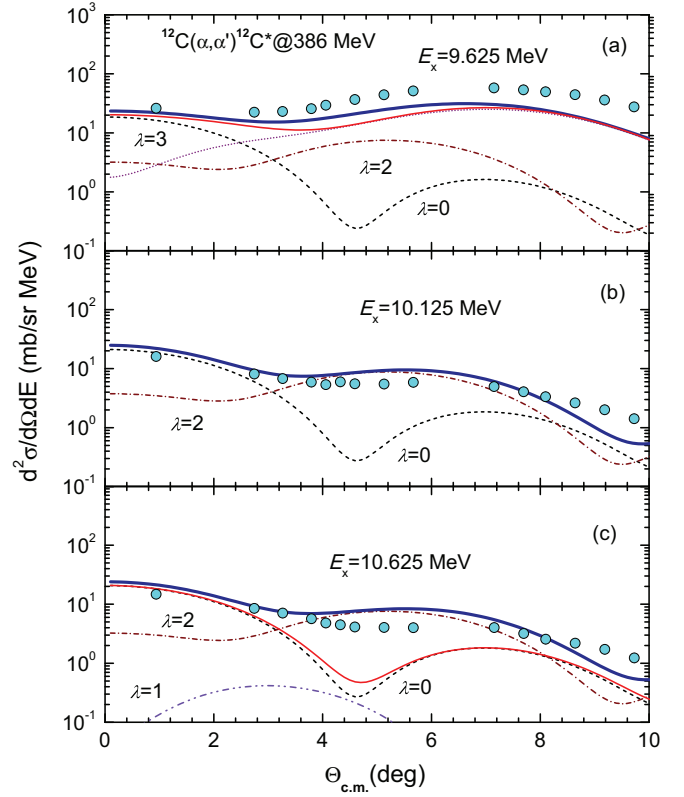
FIG. 13. (Color online) The same as Fig. 12 but with the $E2$ strength of the $2_2^+$ state distributed over a wider energy range spanned by the total width $\Gamma = 2.1$ MeV.

can also be seen in Fig. 11, which consistently confirms our conclusion on the $2_2^+$ peak in the 240-MeV $(\alpha,\alpha')$ spectrum.

The inelastic $\alpha + {}^{12}$C scattering at $E_\alpha = 386$ MeV was measured using the high-precision Grand Raiden spectrometer, and the $(\alpha,\alpha')$ spectrum over the whole energy and angular range has been obtained free of background [22]. In difference from the MDA of the 240-MeV data, the MDA of the 386-MeV data has revealed a clear presence of the $2_2^+$ state at the energy near 10 MeV, and the total $(\alpha,\alpha')$ cross section measured at this energy was used above in our analysis to determine the realistic $E2$ strength of the $2_2^+$ state (see Fig. 9 and the discussion thereafter). With the 386-MeV data available also for many energy bins around $E_x = 10$ MeV, it is of interest to probe the consistency of the present folding-model + CC approach in the calculation of $(\alpha,\alpha')$ scattering at $E_\alpha = 386$ MeV, similar to that shown in Figs. 10 and 11. We note that the $3^-$ transition strength found in the energy bins around 10 MeV by the MDA of the 386-MeV data [22] is better resolved in energy than that found by the MDA of the 240-MeV data [25], and it was used to scale the AMD transition density to obtain the folded $3^-$ inelastic FF of the bin. All the remaining inputs of the folding-model + CC calculation were determined in the same manner as that done above for the 240-MeV data. The CC description of the 386-MeV $(\alpha,\alpha')$ data measured for three similar energy bins around $E_x = 10$ MeV is shown in Fig. 12. One can see that a good overall agreement of our results

with the $(\alpha,\alpha')$ data measured at $E_\alpha = 386$ MeV for these energy bins has been achieved using the same structure inputs for the most important cluster states of $^{12}$C as those used to obtain the CC results shown in Fig. 10. The CC results for the same three energy bins obtained with the $E2$ strength of the $2_2^+$ state distributed over a wider energy range spanned by the total width $\Gamma = 2.1$ MeV are shown in Fig. 13, and one can also see a good agreement of the CC results with the data, especially a better CC description of the data taken for the energy bin centered at $E_x = 10.125$ MeV. This result might well indicate that the $2_2^+$ state has indeed a wide total width $\Gamma \approx 2$ MeV.

## IV. SUMMARY

The complex OP and inelastic scattering FF given by the double-folding model using the nuclear densities predicted by the AMD approach and the CDM3Y6 interaction have been used in the comprehensive CC calculation of the elastic and inelastic $\alpha + {}^{12}$C scattering at $E_\alpha = 240$ and 386 MeV. The $(\alpha,\alpha')$ cross sections calculated in the CC approach for the (IS) cluster states of $^{12}$C are compared with the $(\alpha,\alpha')$ data under study, and the strength of the inelastic FF has been fine tuned in each case to the best CC description of the measured angular distribution to determine the corresponding $E\lambda$ transition strength. A detailed folding-model + CC analysis of the $(\alpha,\alpha')$

data measured in the energy bins around $E_x \approx 10$ MeV has been carried out to reveal the $E2$ transition strength that can be assigned to the $2_2^+$ state of $^{12}$C.

A clear presence of the $2_2^+$ state of $^{12}$C at the excitation energy $E_x \approx 10$ MeV has been confirmed consistently by the present analysis of the $(\alpha,\alpha')$ data measured at $E_\alpha = 240$ and 386 MeV. Given quite strong $E\lambda$ strengths predicted for the $E\lambda$ transitions between the $2_2^+$ state and other cluster states of $^{12}$C, a high-precision $(\alpha,\alpha')$ measurement at the lower beam energy might be an interesting alternative to observe the $2_2^+$ excitation and to probe the indirect (two-step) excitation of this state via the CC scheme shown in Fig. 1.

The obtained best-fit $E\lambda$ strengths of the considered states agree reasonably with the existing database, with the exception of the $B(E2)_{\text{exp}}$ transition rate of the $2_2^+$ state given by the revised analysis of the $^{12}$C$(\gamma,\alpha)^8$Be data [24] that is more than double the best-fit $B(E2)$ value found in our analysis. This result stresses the need for new precise measurements of the excitation of $^{12}$C using the $\alpha$ beam as well as other probes. Some difference between the $E\lambda$ transition strengths of the $0_2^+$, $0_3^+$, $3_1^-$, and $2_2^+$ states given by the present analysis and those given by the earlier multipole decomposition analyses of the same $(\alpha,\alpha')$ data [22,25] has been shown to be attributable, in part, to the strong CC effect and enhanced absorption in the exit channel of the $(\alpha,\alpha')$ scattering.

[1] M. Freer, Rep. Prog. Phys. **70**, 2149 (2007).
[2] Y. Funaki, H. Horiuchi, W. von Oertzen, G. Röpke, P. Schuck, A. Tohsaki, and T. Yamada, Phys. Rev. C **80**, 064326 (2009).
[3] E. Uegaki, S. Okabe, Y. Abe, and H. Tanaka, Prog. Theor. Phys. **57**, 1262 (1977).
[4] M. Kamimura, Nucl. Phys. A **351**, 456 (1981).
[5] R. Pichler, H. Oberhummer, A. Csoto, and S. A. Moszkowski, Nucl. Phys. A **618**, 55 (1997).
[6] A. Tohsaki, H. Horiuchi, P. Schuck, and G. Röpke, Phys. Rev. Lett. **87**, 192501 (2001).
[7] Y. Funaki, A. Tohsaki, H. Horiuchi, P. Schuck, and G. Röpke, Phys. Rev. C **67**, 051306(R) (2003).
[8] M. Chernykh, H. Feldmeier, T. Neff, P. von Neumann-Cosel, and A. Richter, Phys. Rev. Lett. **98**, 032501 (2007).
[9] H. O. U. Fynbo and M. Freer, Physics **4**, 94 (2011).
[10] H. Morinaga, Phys. Rev. **101**, 254 (1956).
[11] Y. Funaki, A. Tohsaki, H. Horiuchi, P. Schuck, and G. Röpke, Eur. Phys. J. A **24**, 321 (2005).
[12] C. Kurokawa and K. Katō, Nucl. Phys. A **738**, 455 (2004).
[13] Y. Kanada-En'yo, Prog. Theor. Phys. **117**, 655 (2007).
[14] E. Epelbaum, H. Krebs, T. A. Lähde, D. Lee, and Ulf-G. Meißner, Phys. Rev. Lett. **109**, 252501 (2012).
[15] M. Freer et al., Phys. Rev. C **76**, 034320 (2007).
[16] C. Aa. Diget et al., Phys. Rev. C **80**, 034316 (2009).
[17] M. Freer et al., Phys. Rev. C **80**, 041303(R) (2009).
[18] T. Muñoz-Britton et al., J. Phys. G **37**, 105104 (2010).
[19] W. R. Zimmerman, N. E. Destefano, M. Freer, M. Gai, and F. D. Smit, Phys. Rev. C **84**, 027304 (2011).
[20] M. Freer et al., Phys. Rev. C **86**, 034320 (2012).
[21] H. Friedrich, L. Satpathy, and A. Weiguny, Phys. Lett. B **36**, 189 (1971).
[22] M. Itoh et al., Phys. Rev. C **84**, 054308 (2011).
[23] W. R. Zimmerman et al., Phys. Rev. Lett. **110**, 152502 (2013).
[24] W. R. Zimmerman, Ph.D. dissertation, University of Connecticut, 2013, http://digitalcommons.uconn.edu/dissertations/230/.
[25] B. John, Y. Tokimoto, Y. W. Lui, H. L. Clark, X. Chen, and D. H. Youngblood, Phys. Rev. C **68**, 014305 (2003).
[26] D. T. Khoa, D. C. Cuong, and Y. Kanada-En'yo, Phys. Lett. B **695**, 469 (2011).
[27] D. T. Khoa and G. R. Satchler, Nucl. Phys. A **668**, 3 (2000).
[28] D. T. Khoa, W. von Oertzen, H. G. Bohlen, and S. Ohkubo, J. Phys. G **34**, R111 (2007).
[29] G. R. Satchler, Direct Nuclear Reactions (Clarendon Press, Oxford, U.K., 1983).
[30] D. T. Khoa, Phys. Rev. C **63**, 034007 (2001).
[31] W. G. Love, Nucl. Phys. A **312**, 160 (1978).
[32] F. Carstoiu and M. Lassaut, Nucl. Phys. A **597**, 269 (1996).
[33] D. T. Khoa, G. R. Satchler, and W. von Oertzen, Phys. Rev. C **56**, 954 (1997).
[34] D. C. Cuong, D. T. Khoa, and G. Colò, Nucl. Phys. A **836**, 11 (2010).
[35] J. P. Jeukenne, A. Lejeune, and C. Mahaux, Phys. Rev. C **16**, 80 (1977).
[36] D. T. Khoa and D. C. Cuong, Phys. Lett. B **660**, 331 (2008).
[37] D. T. Khoa, Int. J. Mod. Phys. E **17**, 2055 (2008).
[38] M. N. Harakeh and A. E. L. Dieperink, Phys. Rev. C **23**, 2329 (1981); N. V. Giai and H. Sagawa, Nucl. Phys. A **371**, 1 (1981).
[39] S. Raman, C. W. Nestor, Jr., and P. Tikkanen, At. Data Nucl. Data Tables **78**, 1 (2001).
[40] P. Strehl, Z. Phys. **234**, 416 (1970).
[41] P. M. Endt, At. Data Nucl. Data Tables **23**, 3 (1979); F. Ajenberg-Selove, Nucl. Phys. A **506**, 1 (1990).
[42] T. Kibedi and R. H. Spear, At. Data Nucl. Data Tables **80**, 35 (2002).
[43] Th. Neff (private communication).
[44] H. Feshbach, Theoretical Nuclear Physics Nuclear Reactions (Wiley, New York, 1992).
[45] J. Raynal, in Computing as a Language of Physics (IAEA, Vienna, 1972), p. 75; CC code ECIS97 (unpublished).
[46] A. Ingemarsson, J. Nyberg, P. U. Renberg, O. Sundberg, R. F. Carlson, A. J. Cox, A. Auce, R. Johansson, G. Tibell, D. T. Khoa, and R. E. Warner, Nucl. Phys. A **676**, 3 (2000).
[47] G. R. Satchler and D. T. Khoa, Phys. Rev. C **55**, 285 (1997).
[48] B. John, X. Chen, and D. H. Youngblood (private communication).